A Machine Learning Based Fast Forward Solver for Ground Penetrating Radar with Application to Full Waveform Inversion

Iraklis Giannakis, Antonios Giannopoulos, and Craig Warren

***Abstract*—The simulation, or forward modeling, of Ground Penetrating Radar (GPR) is becoming a more frequently used approach to facilitate interpretation of complex real GPR data, and as an essential component of full-waveform inversion (FWI). However, general full-wave 3D electromagnetic (EM) solvers, such as ones based on the Finite-Difference Time-Domain (FDTD) method, are still computationally demanding for simulating realistic GPR problems. We have developed a novel near real-time, forward modeling approach for GPR that is based on a machine learning (ML) architecture. The ML framework uses an innovative training method which combines a predictive principal component analysis technique, a detailed model of the GPR transducer, and a large dataset of modeled GPR responses from our FDTD simulation software. The ML-based forward solver is parameterized for a specific GPR application, but the framework can be applied to many different classes of GPR problems.**

To demonstrate the novelty and computational efficiency of our ML-based GPR forward solver, we used it to carry out FWI for a common infrastructure assessment application – determining the location and diameter of reinforcement bars in concrete. We tested our FWI with synthetic and real data, and found a good level of accuracy in determining the rebar location, size, and surrounding material properties from both datasets. The combination of the near real-time computation, which is orders of magnitude less than what is achievable by traditional full-wave 3D EM solvers, and the accuracy of our ML-based forward model is a significant step towards commercially-viable applications of FWI of GPR.

***Index Terms*—Concrete, Deep learning, FDTD, FWI, GPR, Machine Learning, NDT, Neural Networks, Rebar**

I. Introduction

Ground Penetrating Radar (GPR) is a non-destructive electromagnetic (EM) tool that is commonly used for infrastructure assessment and geophysical investigations. The simulation, or forward modeling, of GPR is now more frequently carried out for two primary reasons: firstly, as a tool to assist with the interpretation of, often complex, real GPR data; and secondly, because an accurate and fast forward model is a key component in the full-waveform inversion (FWI) of GPR data. There have been recent advancements in the capabilities and accuracy of GPR simulations [1], [2], as well as improvements to the performance of the software. Nevertheless, full-waveform three dimensional (3D) EM forward solvers, like the Finite-Difference Time-Domain (FDTD) method, remain computationally demanding algorithms. This is especially challenging for FWI, particularly when global optimizers are used, where the forward problem has to be evaluated hundreds, if not thousands, of times. To attempt to mitigate this, simplifications of the forward model have been proposed, such as 3D to two dimensional (2D) transformations, and the use of simplified GPR antenna models [3], [4]. However, when targets are located in the near or intermediate field of the GPR antenna these methods do not produce sufficiently accurate results. Therefore FWI algorithms that use realistic and accurate 3D forward models have only been used where high-performance computing (HPC) resources are available. This has led to extremely limited mainstream/commercial adoption of FWI for GPR.

We propose a novel near real-time 3D forward model for GPR based on machine learning (ML). One of the most mainstream ML methods are neural networks, which have been extensively used in a wide range of applications [5]. Deep networks are theoretically capable of resolving highly complicated patterns in multi-dimensional spaces when adequate training data are available. Nonetheless, training a deep architecture using traditional neural networks is not a straightforward task, and for many years neural networks were constrained to use a maximum of three hidden layers [5]. Recent advancements in ML make it possible to train deep architectures by using a new spectrum of neural networks like convolutional neural networks, long-short term memory networks, and neural networks that use initial weights obtained from pre-trained unsupervised learning (e.g. using auto-encoders) [6]. In addition, training techniques like the dropout [7], rectified linear unit activation functions [8], and stochastic optimization approaches [9] manage to reduce over-fitting allowing deep architectures to be effectively trained.

The initial kernel for our ML approach was developed in [10], where we accurately predicted the direct coupling response of a GPR antenna for specific soil parameters based on the Peplinksi model [11], the height of the antenna, and the roughness of the surface. A similar concept has also been proposed to estimate the arrival times in 2D ray-based tomography [12]. However, our initial approach could not predict the response from a buried target with sufficient accuracy. This is because the complex interactions between the target and the surface, combined with ringing noise and losses give rise to a multi-parametric scenario that neural networks,

I. Giannakis and A. Giannopoulos are with the School of Engineering, The University of Edinburgh, Edinburgh, EH9 3FG, UK. E-mail: i.giannakis@ed.ac.uk and a.giannopoulos@ed.ac.uk

C. Warren is with the Department of Mechanical and Construction Engineering, Northumbria University, Newcastle, NE1 8ST, UK. E-mail: craig.warren@northumbria.ac.uk .

even with deep architectures, could not capture. The new ML-based approach we present here is capable of predicting the complex interactions between the target, the free surface, and the antenna, subject to realistic dispersive losses. The concept is based on parameterizing the GPR model and using an innovative training technique for the neural network, that is then used to predict the resulting waveform based on those parameters. The training process combines two important features: firstly, it utilizes principal component analysis (PCA); and secondly, it uses a comprehensive and realistic training dataset generated from our FDTD-based simulation software. PCA tries to find an orthonormal hyper-plane in which the data can be mapped using a small number of axes, named principal axes or principal components. It has been successfully applied to GPR as a means to eliminate direct coupling and the ground reflection [13], [14], [15]. Although PCA has been used for clutter reduction in GPR its primary purpose is to compress and reduce the dimensionality of data [16]. We use an innovative predictive PCA for training our neural network. Although generating the training data and training the neural network is a computationally intensive process, it takes place only once. The resulting trained network can be used with near real-time speed ($\approx$ 1 sec) as a forward solver. Obviously the ML-based forward solver is only applicable to a subset of the scenarios it was trained for. However, there are many specific GPR applications where one can effectively limit the range of expected variations and thus specify suitable training models.

A real-time forward solver is a powerful asset that can have applications in many areas of GPR. In particular, FWI can greatly benefit from a fast forward solver since traditional solvers like FDTD are time consuming algorithms which necessitate substantial computational resources. In this paper, FWI coupled with our proposed ML-based numerical framework is applied for estimating the depth and the radius of metallic rebars inside concrete slabs. This application was chosen based on the fact that the problem can be effectively parameterized, and that estimating the radius of the rebar is a challenging problem for which no conclusive approach has yet been reported.

It is well known that GPR has been extensively used for non-destructive testing problems [17], [18], [19] with mainstream civil engineering applications that include: mapping of utilities [20], [21], bridge evaluation [22], [23], road inspection [24], [25], [26], pipe location, [27], [28] and crack detection [29], [30]. The mapping of reinforcement in concrete using GPR [31] is particularly attractive due to the high contrast in dielectric properties between concrete and steel, combined with the fact that concrete is a relatively homogeneous medium which further increases the overall signal-to-clutter ratio. Despite this popularity, estimation of the location and, especially, the diameter of rebar in concrete remains a challenging problem for which there is not yet a conclusive approach. In [32] a novel technique is suggested to estimate the radius of rebar based on post-processing raw data. Initially hyperbola fitting is applied in an effort to obtain the permittivity of the concrete. Furthermore, the ratio between the amplitudes measured in different antenna positions is used in order to evaluate the effective conductivity. Subsequently, a parametric study is conducted using a ray-based forward solver in order to establish a relationship between the maximum amplitude of the reflected signal with respect to conductivity, permittivity, depth, and radius of the rebar. A set of 81 models is evaluated and polynomial fitting is used in order to establish a relationship between the reflected amplitude and the radius of the rebar. This method does not take into account either the directivity pattern of the antenna, or the fact that the pattern is medium-dependent [33]. Furthermore, near-field phenomena, such as coupling effects and ringing noise, can strongly affect the estimation of conductivity, permittivity, as well the dependence of the reflected signal on the radius of the rebar. In [34] a different approach is proposed that is based on the coefficients of power reflectivity combined with an empirical evaluation of the radius of the rebar based on the width of the reflectivity pattern. Similar to [32], the method suggested in [34] does not take into account the antenna, assumes a uniform directivity pattern, no ringing noise, and an absence of coupling affects. In [35], synthetic measurements over steel rebars are conducted, and an investigation of two different polarizations, and the dependence on depth and the radius of the rebar is carried out. This method, similar to the aforementioned ones, is evaluated for a specific host medium and uses simplified transmitters and receivers with no conclusive results. In [36] a discrete and stationary wavelet transform is used in order to estimate the diameter of the rebar assuming that the velocity of the medium is known. Direct knowledge of the velocity of the host medium also allows the usage of hyperbola fitting, with the radius of the rebar as the only unknown [37]. In [38] it is shown that using a Kirchoff-based linearized inversion can effectively recover some information regarding the shape of the targets regardless of the medium velocity. In the same context, a FWI approach is suggested in [39] to estimate the host medium properties and the size and depth of a steel rebar. The suggested inversion assumes a simplified source but the source wavelet is one of the unknowns and is evaluated through a deconvolution in each iteration step. The permittivity and conductivity are also calculated in different steps avoiding imbalances due to sensitivity differences. The misfit is calculated for specific frequencies in order to reduce the computational cost. A shuffled complex evolution is employed to minimize the residuals between the predicted and the actual waveform. The validity of the algorithm is evaluated with synthetic data in which the SCE is shown to be capable of accurately retrieving the dielectric properties of the medium as well as the size and the depth of the rebar. The method is a robust and systematic approach for automatic evaluation of the size of the rebar using all the available information of the waveform with minimum simplifications. Nonetheless, the absence of an actual antenna decreases somewhat the general applicability of the approach. In addition, wavelet estimation based on deconvolution is an ill-posed problem that without any regularization can lead to non-unique results [40]. Lastly, the forward-solver, is still a time-consuming routine that, when coupled with a global optimizer, greatly increases the computational requirements of the inversion.

We aim to develop and apply our ML-based forward solver as part of a FWI to estimate the cover depth and diameter

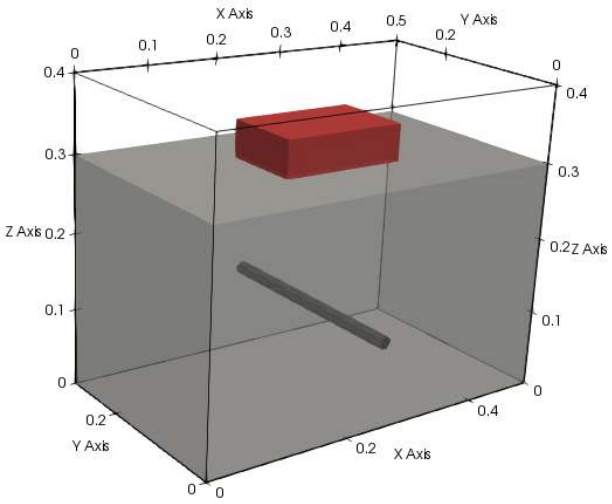

Fig. 1. Diagram showing the geometry of the GPR model used for training the ML-based forward solver (axes values are in metres). The antenna model is within the red box, and the cylindrical object is the PEC rebar.

of rebar, as well as the moisture content of the concrete. A near real-time or very fast numerical solver reduces the computational requirements of FWI making global optimizers usable on computers with modest resources.

II. ML-BASED FORWARD SOLVER

A. Training using FDTD simulations

A training set should include a wide spectrum of possible scenarios in order to adequately map the feature space of a given problem [5]. To achieve this we used numerical modeling to obtain synthetic, but nonetheless realistic and most importantly well-labeled data [41], [42]. Our forward solver used to generate the training data is gprMax [1], which is an open source electromagnetic simulation software based on the FDTD method [43]. gprMax has recently been upgraded to allow the FDTD solver to be executed on multiple graphical processing units [2], which significantly accelerated the generation of the training set. A 1 mm cubic cell is used as a spatial discretization for the FDTD models, and the time-step is set equal to the Courant limit ($\Delta t = 1.925$ ps) [44]. The dimensions of the models are $0.5 \times 0.3 \times 0.4$ m.

The dielectric properties of concrete are described by the extended Debye model given in (1)

$$\epsilon = \epsilon_\infty + \frac{\epsilon_s - \epsilon_\infty}{1 + j\omega t_0} + \frac{\sigma}{j\omega\epsilon_0} \tag{1}$$

where ϵ_∞ is the relative permittivity at infinite frequency, ϵ_s is the relative permittivity at zero frequency, t_0 is the relaxation time, σ is the conductive term, ω is the angular frequency, $j = \sqrt{-1}$, and ϵ_0 is the absolute permittivity of vacuum. A piece-wise linear recursive convolution is used to implement the Debye properties in FDTD model [45]. The properties of the extended Debye model for concrete are given in Table I and were calculated using experimental measurements [46], [47], [48]. A spline interpolation is used to evaluate the parameters for any water fraction between 0.2-12 %. Describing the dielectric properties of concrete using only water fraction is particularly useful for FWI since there is only one unknown parameter to be estimated instead of three. It also overcomes the problem of instabilities due to differences in sensitivity between permittivity and conductivity [49], [50]. This is the reason why a two-step procedure is used in the FWI by [39] (similar to that of [50]), in which an initial permittivity is estimated and subsequently, subject to the derived permittivity an optimized conductivity is calculated. Relating the dielectric properties to the water fraction overcomes these aforementioned instabilities, and furthermore accelerates the overall inversion process.

TABLE I
EXTENDED DEBYE PROPERTIES OF CONCRETE [46]

WC	ϵ_s	ϵ_∞	t_0	σ $(\Omega^{-1}m^{-1})$
12 %	12.84	7.42	0.611 ns	20.6×10^{-3}
9.3 %	11.19	7.2	0.73 ns	23×10^{-3}
6.2 %	9.14	5.93	0.8 ns	6.7×10^{-3}
5.5 %	8.63	6.023	1 ns	5.15×10^{-3}
2.8 %	6.75	5.503	2.28 ns	2.03×10^{-3}
0.2 %	4.814	4.507	0.82 ns	6.06×10^{-4}

The GPR antenna used in the FDTD simulations is a modeled version of the Geophysical Survey Systems Inc. (GSSI) 1.5 GHz antenna, which was also used for collecting measured real data. This model was initially created by [51], where the geometry of the antenna was measured, and a Taguchi optimization was subsequently used in order to derive unknown dielectric properties of the antenna. A cost function of the difference between real and modeled free-space cross-talk responses was used. This antenna model has subsequently been revised and improved by [40], where a hybrid linear/non-linear inversion was employed in order to include the excitation waveform in the unknowns. Through this procedure an optimized pulse is derived simultaneously with the dielectric properties of the antenna. This updated and improved model of the GSSI 1.5 GHz [40] is used in the FDTD simulations for generating the training data.

The rebar is modeled as a perfect electric conductor (PEC) cylinder with a radius varying from 2-25 mm, and with a cover depth that could vary from 0-300 mm. The polarization of the antenna model is parallel to the main axis of the rebar. Figure 1 gives a general overview of the typical geometry of the FDTD models used for the training process.

The training set consisted of 2000 models based on a random variation of the following parameters:

- Water fraction of the concrete (WC)
- Radius of the rebar (R)
- Depth of the rebar (D)

The post-trained neural networks use the aforementioned parameters as inputs in order to predict the resulting waveform in near real-time (≈1 sec).

B. Principal Component Analysis (PCA)

Principal Component Analysis (PCA) is one of the oldest representation techniques used to reduce the dimensionality of ML problems [16], and is a key aspect of our proposed

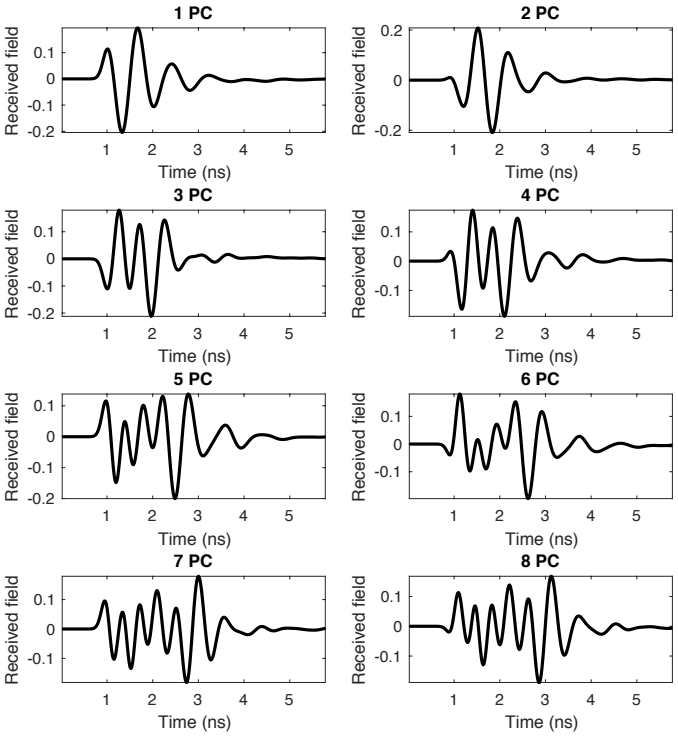

Fig. 2. Eight most dominant principal components of the training set.

ML-based forward solver. The training data consisted of 2000 measurements each of which contained 3000 time-steps. Since the FDTD time-step is 1.925 ps and we do not expect to have useful information at frequencies >7 GHz, the traces were under-sampled in time domain to accelerate the training process and reduce the overall computational requirements. Thus, the training set can be represented by a matrix $\mathbf{T} = [\mathbf{tr}_1,\ \mathbf{tr}_2\ ...\ \mathbf{tr}_m] = T_{i,j} \in \mathbb{R}^{m\times n}$, where $m = 2000$ is the total number of models (A-Scans), $n = 300$ are the under-sampled time-steps, and $\mathbf{tr}_i$ is the under-sampled trace. The principal components of $\mathbf{T}$ are 300 vectors, and can be represented in a matrix form as $\mathbf{P}= P_{i,j} \in \mathbb{R}^{n,n}$. Figure 2 shows the eight dominant principal axes of the training set to illustrate the components in which the signal is decomposed. The full signal consists of 300 components, but to illustrate the concept we show only the 8 most dominant ones here. A linear combination of the principal axes can exactly replicate any trace in the training set. Thus, any trace can be calculated through $\mathbf{tr}_i = \mathbf{P}\mathbf{w}_i$, where $\mathbf{w}_i$ is a vector containing the eigenvalues of the ith trace. When using all the principal axes the system is well-determined and the solution is exact. Choosing a subset of principal axes $\mathbf{Q} \in \mathbb{R}^{n,v}$ $(n > v)$ results in an over-determined system that can be solved using least squares $\mathbf{w}_i = \left(\mathbf{Q}^T\mathbf{Q}\right)^{-1}\mathbf{Q}^T\mathbf{tr}_i$. By doing so, the data can be represented by a smaller amount of unique linear coefficients multiplied by a common set of principal axes. This results in decreasing the dimensionality with the cost of losing the information contained in the neglected principal components. For the present problem, using 40 principal components was found to be sufficient to represent any given trace of the set. Figure 3 shows the average absolute error between the actual and the compressed normalized traces with respect to the number of principal axes used to approximate the data.

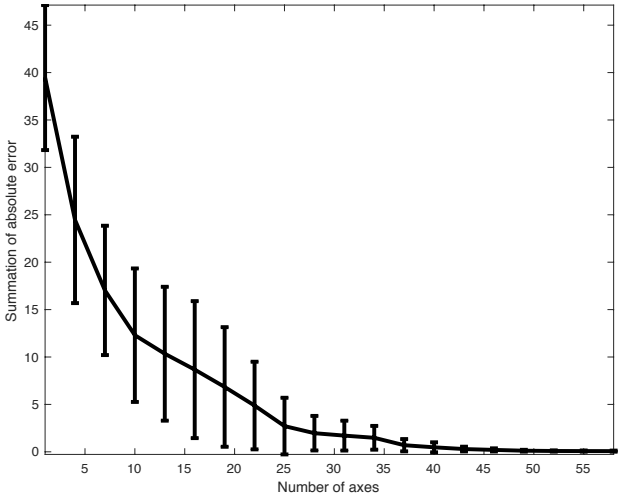

Fig. 3. Average error between the actual and the compressed normalized A-Scans. The error is plotted with respect to the number of principal axes used in the compression. The error bars correspond to one standard deviation.

Using the 40 most dominant principal axes, the training set can be represented by a matrix $\mathbf{W} = W_{i,j} \in \mathbb{R}^{m,N}$ where $N = 40$ is the number of linear coefficients that uniquely define each trace. Figure 4 shows three full A-Scans calculated using FDTD and their corresponding compressed PCA representations using 40 principal axes. From 3000 time-steps the data have been compressed without compromising the overall accuracy to a set of 40 coefficients that are unique for each trace. Based on the inputs of the model (WC, R, D) the vector $\mathbf{w}_i$ will be the final output of the ML-based forward solver that will subsequently be decompressed to retrieve the complete A-Scan.

C. Design of the network architecture

Supervised ML tries to establish a causal relationship between given inputs and their corresponding outputs. As already mentioned, in the current problem the inputs are the water content of the concrete (WC), the radius of the rebar (R), and the depth of the rebar (D). Initially, it was attempted to establish a relationship between the given inputs and the actual A-Scans, subject to the 2000 randomly generated scenarios. Following that approach the resulting outputs were very noisy and the late reflections, ringing noise, and complicated near-field phenomena could not be predicted regardless of the neural network architecture. Subsequently, an attempt was made to establish a relationship between the given inputs and the 40 unique principal components of each trace. Similarly to the first direct approach, the neural network could not predict the complicated phenomena, and it was only possible to resolve the direct coupling. Note that a number of different neural network architectures, different activation functions, as well as different optimization approaches were tested producing no satisfactory results.

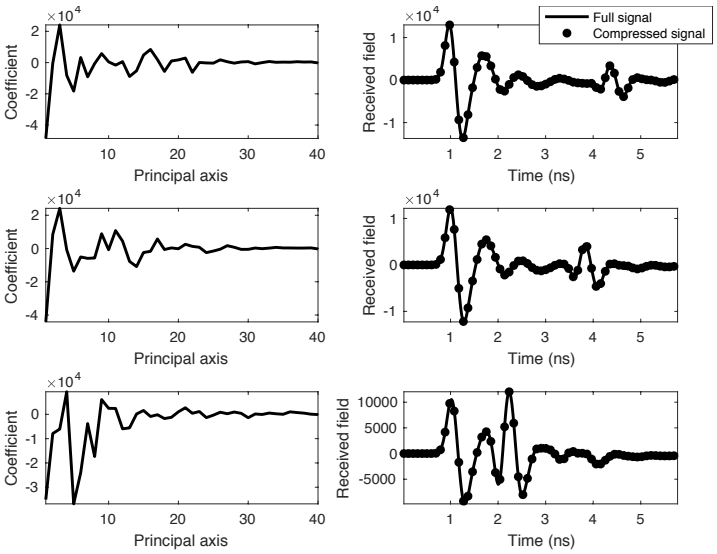

Fig. 4. Left column: 40 principal coefficients used to represent the compressed signal. These are the outputs of the ML-based numerical solver which are subsequently decomposed to form the resulting signal. Right column: Three full A-scans calculated using FDTD and their corresponding compressed PCA representations using 40 principal components.

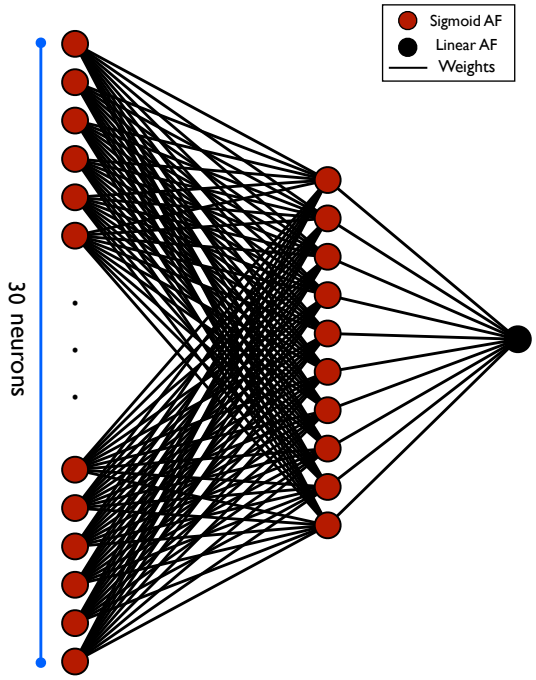

Fig. 5. Neural network architecture used in each step of the proposed ML-based forward solver. All the activation functions (AF) are sigmoid apart from the last one which is linear.

It is apparent that scattering from a PEC rebar in the close proximity to an actual GPR antenna is a complicated problem that requires a deep architecture specifically designed for the problem. The main design idea of our proposed architecture is to try and exploit the fact that the principal components are not independent from each other, and that knowing the values of the previous ones should assist in predicting the next ones. Figure 4 shows that the principal components follow a specific pattern that can be approximately described as a periodic function with an exponential decay.

Our proposed neural architecture is divided into two sections, with each section further divided into 40 steps. In the first section the inputs of the model ($R,\ D,\ WC$) are used in order to predict the first principal axis. The neural network architecture used is a two hidden layers model using 30 and 10 neurons respectively. The activation functions of the neurons are sigmoid apart from the output which is linear, as shown in Figure 5. This architecture is used in each step of the proposed algorithm. For the training process, the data are divided into three sets: a training set, a validation set, and a testing set. The training set is used to calculate the gradients and the cost function of the optimization. The validation set is used as a flag in order to stop the process when the system starts to overfit. Lastly, the testing set is used to evaluate the performance of the resulting neural network. The optimization used for the current problem is a complex-conjugate gradient method.

The first step of the first section results in a system that uses the parameters of the model as inputs in order to predict the first principal component. Subsequently, the parameters of the model plus the predicted value of the first component are used to predict the value of the second principal component (using the neural network described in Figure 5). The causal relationship between the principal components constrains the possible outcomes thus decreasing the search space of the optimization. In the third step, the parameters of the model are used in addition to the previously predicted principal components (i.e. both the first and the second one) in order to predict the third one. This procedure is continued until all 40 of the components have been predicted. Note that each step is trained individually, thus avoiding vanishing gradients and over-fitting that arise when training deep architectures. In addition, in each step, the data are divided into different training, validation, and testing sets which decreases overfitting by forcing the neural network to be inclusive and not biased to a specific set of data. Figure 6 provides an overview of the architecture of the first section, where each box contains the neural network architecture presented in Figure 5. The first section is a 120 layer neural network in which every three layers are trained individually using the parameters of the model plus the outputs of the previous steps.

After the evaluation of the first section, a full set of predicted principal components are available. These coefficients are subject to errors due to inaccurate predictions. To overcome this, a second section is introduced which tries to establish a causal relationship between the errors in the predicted values with respect to the actual principal axes and the parameters of the model. In the first step of the second section, the parameters of the model plus all the predicted principal components apart from the first one are used in order to predict the revised first principal axis. The same neural network described in Figure 5 is used for all the steps in the second section, similar to the first section. During the second step, the parameters of the model and the revised first component together with all the predicted components from the first section apart from the second one

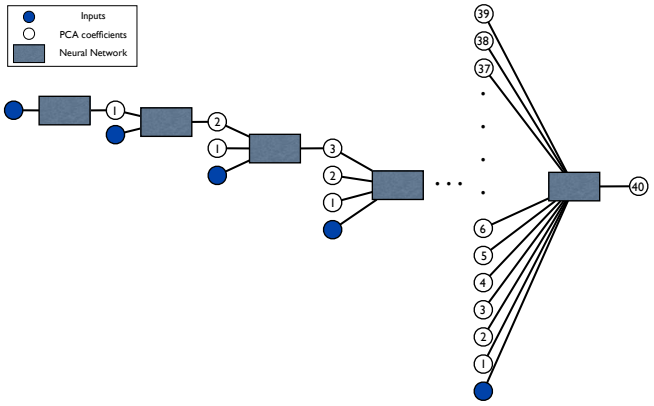

Fig. 6. The architecture of the first section of the proposed ML-based forward solver. Each box corresponds to the neural network in Figure 5. The network is a 120 layers deep and each step is trained individually using the outputs of the previous layers as inputs plus the parameters of the model.

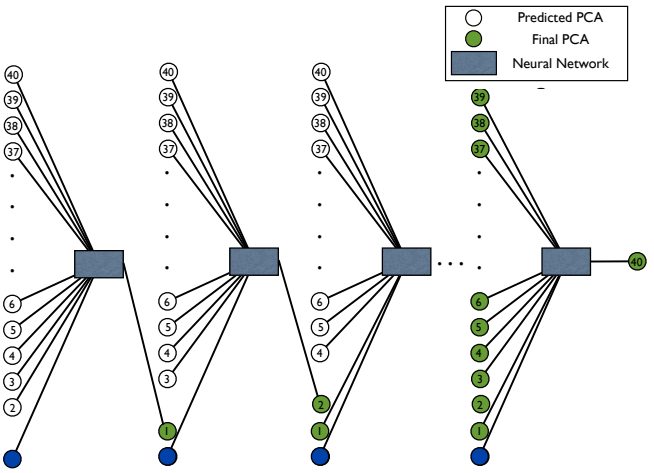

Fig. 7. The architecture of the second section of the proposed ML-based forward solver. The boxes correspond to the neural network described in Figure 5. In each step the predicted values of the first section (Figure 6) plus the revised values of the previous steps, and the parameters of the model are used as inputs in order to revise the next principal component.

are used to predict the revised second principal component. The same procedure is repeated until all the components are successfully revised. Figure 7 presents the architecture of the second section which follows the first one in a sequential manner. Similarly to the first section, each step of the second section is trained individually using as inputs the parameters of the model and the outputs of the first section and the outputs of the previous steps of the second section. Again, in each step the training set is divided in different training, validation, and testing sets that furthermore reduces over-fitting.

The final neural network architecture including the first section and the second section with all their steps, consists of 240 layers. Although generating the training set and tuning the suggested neural network is computationally intensive, the final output is a near real-time ($\approx$ 1 sec) estimator of the 40 principal components that can be decompressed to give the predicted time-domain modeled GPR A-Scan. Notice that the proposed neural network uses as inputs the predicted principal

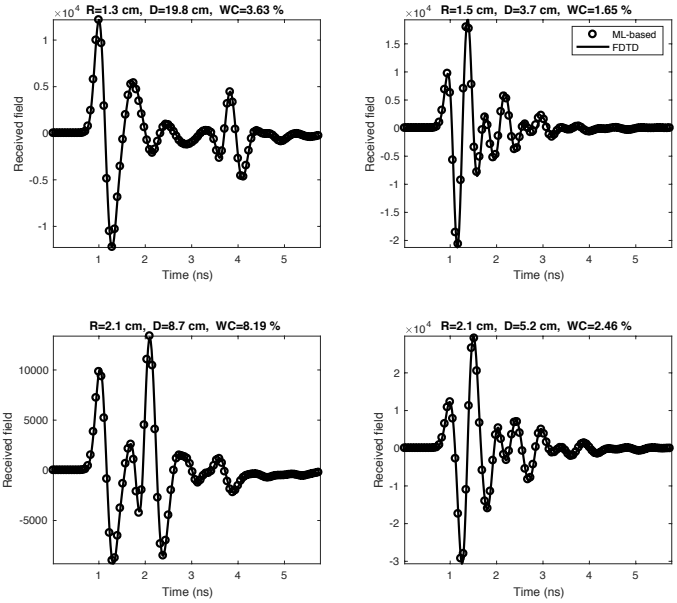

Fig. 8. Four different cases used to compare the proposed ML-based solver with the FDTD solver. The inputs of the model – rebar radius, rebar depth, and water content of the concrete – are given as the title of each subplot.

components and not the actual ones. The only inputs required from the user are values for the water content of the concrete, and the radius and cover depth of the rebar.

The accuracy of the ML-based forward solver is demonstrated in Figure 8, which presents four case studies that compare A-Scans from the ML-based forward solver with ones obtained directly using the FDTD forward solver. The results are almost identical showing that the suggested neural network architecture can resolve the underlying pattern between the given inputs and their corresponding A-Scans.

D. Generalization capabilities

The proposed ML-based numerical solver has been trained for the GSSI 1.5 GHz commercial antenna. In addition, the current scheme is tuned for predicting the resulting signal of a metallic rebar buried in concrete. It is apparent that the architecture described in Figure 7 is not capable of predicting the response produced using other antenna systems in different environments. Applying deep learning to simulate different scenarios will result in a different network architecture, which in turn will require different training strategies and different training sets. There is neither a universal method to train neural networks for electromagnetic simulations, nor an inclusive neural network that can replace Maxwell's equations. The ML-based solver described in this section is specifically designed for the GSSI 1.5 GHz commercial antenna used on concrete with different water content and buried rebar with different depths and radii.

III. FWI RESULTS

We now apply our ML-based forward solver as part of a FWI to estimate the cover depth and diameter of rebar, as well as the moisture content of the concrete. A simulated annealing

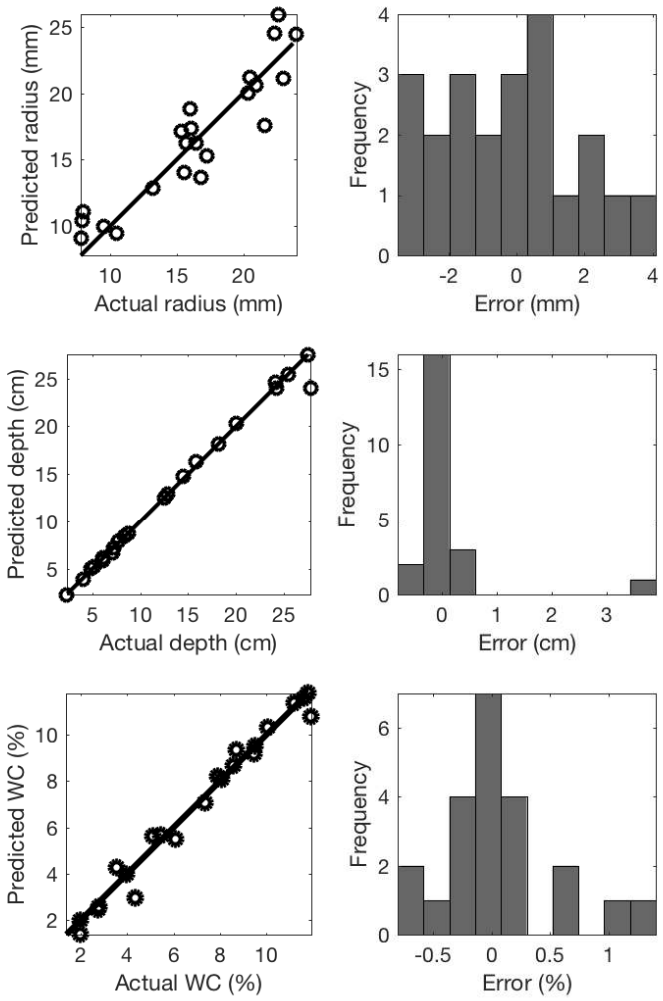

Fig. 9. Actual and predicted parameters using FWI and our ML-based solver. The numerical study includes 21 models. The frequency of occurrence with respect to error is plotted on the right side. The depth of the rebar and the water content of the concrete can be accurately predicted. Due to the frequency content of the pulse as well as due to the inherent non-uniqueness of the problem, the radius of the rebar can be obtained with a maximum error of 6 mm.

optimization [52] is used in order to minimize the average mean absolute error between the modeled, using the ML-based forward solver, and the objective traces. A global optimizer can constrain the model to exist within given boundaries, which is particularly useful since our ML-based forward solver has been trained for a specific set of cases ($R = 2{-}25$ mm, $D = 0{-}300$ mm, $WC = 0.2{-}12$ %). Trying to estimate resulting A-Scans for values outside these predefined boundaries, will result in unreliable extrapolations, and should be avoided.

Global optimizers can overcome local minima that are present in FWI problems in electromagnetics. In addition, using global optimizers makes initialization of the problem unnecessary, thus avoiding ray-based tomography inversion prior to FWI. The main drawback of global optimizers is that they require substantially more computational resources compared to convex optimizers. Our ML-based numerical scheme, is a near real-time solver with minimum computational requirements. This makes the usage of global optimizers attainable

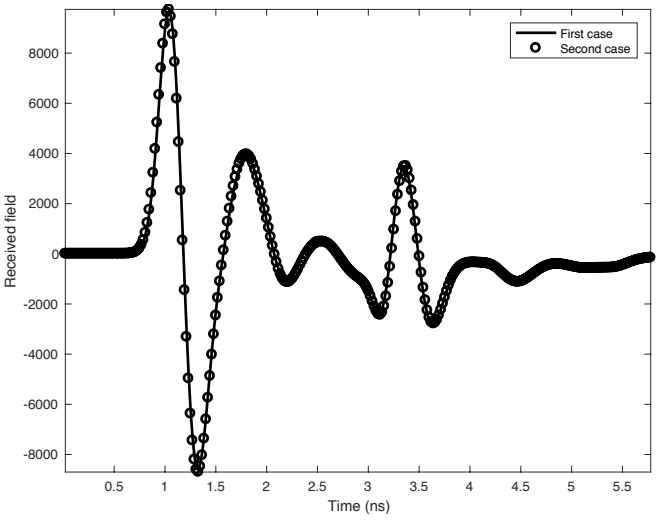

Fig. 10. Two case studies presented in order to illustrate the inherent non-uniqueness of the rebar problem. For the first case the water content of the concrete is $WC = 9.7$ %, the rebar has $R = 25.53$ mm radius, and a depth of $D = 161.1$ mm. For the second case, $WC = 9.5$ %, $R = 18.8$ mm, and $D = 155.4$ mm.

and commercially appealing. Although in the current work the chosen global optimizer is the simulated annealing, the proposed numerical solver can be applied in a straightforward manner using other global optimizers like genetic algorithms, and particle swarm optimization.

A. Synthetic data

The proposed FWI using our novel ML-based forward solver was first tested with 21 synthetic datasets. The cases were randomly selected and the results of the FWI are shown in Figure 9. The depth of the rebar as well as the water content of the concrete can be accurately predicted. The radius of the rebar can be obtained with a maximum error of about 6 mm. The reason for this error is the inherent non-uniqueness of the problem (i.e. different models can result in similar A-Scans) illustrated in Figure 10. This occurs because the frequency content of the pulse is not adequate to resolve differences of the order of 6 mm in a low dielectric medium such as concrete. Nonetheless, given the efficiency of the current method in the field as it only requires a single measurement, and the minimum computational requirements, a maximum error of 6 mm is a good approximation that could be considered useful for a number of applications. No initialization is required from the user, nor any calibration of the GPR antenna. A single trace over the investigated position is the only necessary input.

B. Real data

The proposed methodology is an attractive method for mainstream/commercial applications with real GPR data, due to its efficiency and degree of automation. Nonetheless, the suggested technique uses a ML-based forward solver that has been trained using synthetic data, so any discrepancies between real and synthetic data used in the FDTD training can affect the overall accuracy of the FWI scheme. To minimize

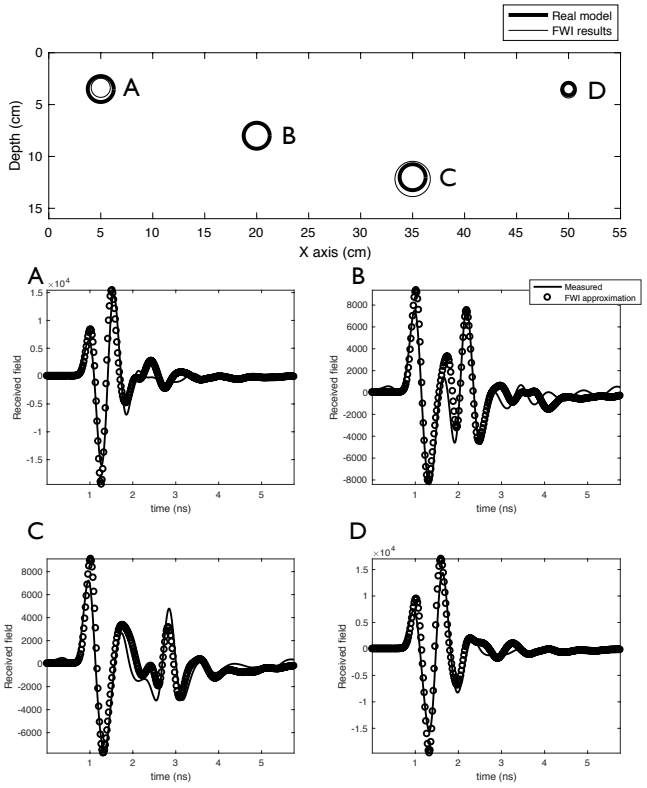

Fig. 11. FWI results for real measurements over four rebars with different radii and depths. The recovered water content of the concrete is approximately 11.5 %.

these effects, special attention was given to simulate the GSSI 1.5 GHz antenna used in the training as realistically as possible [40], and likewise in modeling the dielectric properties of concrete [46].

Four case studies were examined using data collected from a reinforced concrete slab in the Non-Destructive Testing laboratory at the School of Engineering, The University of Edinburgh. The measurements were taken using a GSSI 1.5 GHz antenna over four different steel rebars in a well-cured concrete slab ($>$ 3 years). The measurements were made directly above each rebar, with the polarization of the antenna parallel to the longitudinal axis (as Figure 1). Similarly to [40], filters for the antenna on the GPR system were disabled in order to record the raw antenna response. The only post-processing applied was the removal of low frequency (static) phenomena that can be approximated with a second order polynomial [40]. The resulting water fraction from the FWI was approximately 11.5 %. The estimated and the actual depths and radii of the rebars are shown in Figure 11. The predicted and the actual rebar characteristics are in good agreement indicating the usefulness and the potential of the proposed methodology for field applications.

IV. Conclusions

A novel forward solver based on machine learning (ML) for Ground Penetrating Radar (GPR) has been developed that can be executed at near real-time speeds ($\approx$ 1 sec), overcoming the computational costs of more general full-wave three dimensional (3D) numerical solvers like the Finite Difference Time Domain (FDTD) method. The approach is based on innovative training of a deep neural network through a combination of predictive principal component analysis, and a comprehensive training dataset using realistic data from representative 3D FDTD simulations. As a result, for the first time, a near real-time forward solver makes full waveform inversion (FWI) using global optimizers attainable on standard desktop/laptop computers. Using global optimizers tackles the problem of local minima that are widely present in FWI problems in electromagnetics. In addition, global optimizers do not require initialization from the user, thus making the procedure fully automatic. A simulated annealing optimization is employed in order to minimize the mean absolute error between the real and the synthetic traces. Through numerical and real experiments it is shown that, for the given antenna, the position of the rebar and the water content of the concrete can be readily obtained, and the radius of the rebar can be estimated with a maximum error of $\approx$ 6 mm. The proposed methodology provides fast and accurate results using a single trace measured over the investigated rebar. These benefits make our approach very attractive for field applications, and a step forward in making FWI commercially viable.

The concept of using ML to create a forward electromagnetic solver for GPR is not a solution to the general GPR modeling problem, and consequently we do not suggest that this approach makes general FWI feasible, without any prior information or constraints. However it is clear that there are classes of GPR problems (where the forward model can be adequately parametrized) that the proposed ML-based approach can be successfully applied. An example of such a type of scenario is the assessment of pavements with GPR, where the forward model is essentially based on a one dimensional layered approximation. Extending our methodology to more complicated scenarios, where multiple scattering events are more important, should be possible and will expand the applicability of the approach. Indeed, our concept can be employed for other electromagnetic sensing applications, that require complex inverse scattering solutions, to reduce the computational demands of forward modeling.

References

[1] C. Warren, A. Giannopoulos and I. Giannakis, "gprMax: Open source software to simulate electromagnetic wave propagation for Ground Penetrating Radar," *Comput. Phys. Commun.* vol. 209 pp. 163-170, 2016.

[2] C. Warren, A. Giannopoulos, A. Gray, I. Giannakis, A. Patterson, L. Wetter and A. Hamrah, "A CUDA-based GPU engine for gprMax: open source FDTD electromagnetic simulation software," *Computer Physics Communications*, 2018, Early Access.

[3] J. Ernst, H. Maurer, A. G. Green and K. Holliger, "Application of a new 2D time-domain full-waveform inversion scheme to crosshole radar data," *Geophysics*, vol. 72, no. 5, pp. J53-J64, 2007.

[4] S. Busch, J. van der Kruk, J. Bikowski, and H. Vereecken, "Quantitative conductivity and permittivity estimation using full-waveform inversion of on-ground GPR data," *Geophysics*, vol. 77, pp. H79-H91, 2012.

[5] M. C., Bishop, *Neural Networks for Pattern Recognition*, Oxford University Press, 1996.

[6] J. Schmidhuber, "Deep learning in neural networks: An overview," *Technical Report IDSIA, arXiv: 1404.7828*, pp. 1-88, 2014.

[7] N. Srivastava, G. Hinton, A. Krizhevsky, I. Sutskever and R. Salakhutdinov, "Dropout: A simple way to prevent neural networks from overfitting," *J. of Machine Learning Research*, vol. 15, pp. 1929-1958, 2014.

[8] Y. LeCun, Y. Bengio and G. Hinton, "Deep learning," *Nature*, vol. 521, pp. 436-444, 2015.

[9] D. Kingma and J. L. Ba, "Adam: A method for stochastic optimization," in *Proc. of ICLR*, pp. 1-15, 2015.

[10] I. Giannakis, A. Giannopoulos and C. Warren, "A machine learning approach for simulating ground penetrating radar," in *Proc. 17th Inter. Conf. on Ground Penetrating Radar*, Rapperswil, 2018, pp. 1-4.

[11] N. R. Peplinski, F. T. Ulaby, and M. C. Dobson, "Corrections to dielectric properties of soils in the 0.31.3-GHz range," *IEEE Trans. Geosci. Remote Sens.* , vol. 33, no. 6, p. 1340, Nov. 1995.

[12] T. M. Hansen and K. S. Cordua, "Efficient Monte-Carlo sampling of inverse problems using neural network-based forward–applied to GPR crosshole traveltime inversion," *Geoph. J. Inter.*, vol. 211, pp. 1524-1533, 2017.

[13] G. B. Kaplan, O. Ioglu, A. B. Yoldemir and M. Sezgin, "Real-time object detection using dynamic principal component analysis," in *Proc. of the 13th Inter. Conference on Ground Penetrating Radar*, Lecce, 2010, pp. 1-6.

[14] E. Tebchrany, F. Sagnard, V. Baltazart, J. P. Tarel and X. Drobert, "Assessment of statistical-based clutter reduction techniques on ground-coupled GPR data for the detection of buried objects in soils," in *Proc. of the 15th Inter. Conf. on Ground Penetrating Radar*, Brussels, 2014, pp. 604-609.

[15] P. Kaczmarek and J. Pietrasinski, "Principal component analysis in interpretation of A-Scan measurements in GPR system," in *Proc. 15th Inter. Radar Symposium (IRS)*, Gdansk, 2014, pp. 1-5.

[16] Y. Bengio, A. Courville and P. Vincent, "Representation learning: A review and new perspectives," *IEEE Trans. on Pattern Analysis and Machine Intelligence*, vol. 35, no. 8, pp. 1798-1828, Aug. 2013.

[17] D. J. Daniels, *Ground Penetrating Radar*, 2nd ed. London, U.K.: Institution of Engineering and Technology, 2004.

[18] A. P. Annan, "GPR-History, trends, and future developments," *Subsurface Sens. Technol. Appl.* , vol. 3, no. 4, pp. 253-270, 2002.

[19] A. Benedetto, F. Tosti, L. B. Ciampoli and F. DAmico, "GPR applications across engineering and geoscience disciplines in Italy: A review," *IEEE J. Sel. Topics Appl. Earth Observ. Remote Sens*, vol. 9, no. 7, pp. 2952-2965, July 2016.

[20] J. L. Porsani, Y. B. Ruy, F. P. Ramos and G. R. Yamamouth, "Gpr applied to mapping utilities along the route of the Line 4 (yellow) subway tunnel construction in Sao Paulo City, Brazil," *J. of Appl. Geoph.*, vol 80, pp. 25-31, 2012.

[21] G. Grandjean, J. C. Gourry and A. Bitri, "Evaluation of GPR techniques for civil- engineering applications: study on a test site," *J. of Appl. Geoph.*, vol 45, pp.141156, 2000.

[22] S. K. Rehman, Z. Ibrahim, S. A. Menmon and M. Jameel, "Nondestructive test methods for concrete bridges: A review," *Constructions and Buildings Materials*, vol. 107, pp. 58-86, 2016.

[23] M. Solla, H. Lorenzo, f. I. Rial and A. Novo, "Ground-penetrating radar for the structural evaluation of masonry bridges: Results and interpretational tools," *Construction and Building Materials*, vol. 29, pp. 458-465, 2012.

[24] M. Solla, X. Nez-Nieto, M. Varela-Gonzlez, J. Martnez-Snchez and P. Arias, "GPR for road inspection: Georeferencing and efficient approach to data processing and visualization," in *Proc. of the 15th Inter. Conf. on Ground Penetrating Radar*, Brussels, 2014, pp. 913-918.

[25] F. Tosti, S. Adabi, L. Pajewski, G. Schettini and A. Benedetto, "Large-scale analysis of dielectric and mechanical properties of pavement using GPR and LFWD," in *Proc. of the 15th Inter. Conf. on Ground Penetrating Radar*, Brussels, 2014, pp. 868-873.

[26] F. M., Fernandes and J. Pais, "Assessment of moisture in road pavements," in *Proc. of the 15th Intern. Conf. on Ground Penetrating Radar*, Brussels, 2014, pp. 909-912.

[27] A. Risti, M. Vrtunski, M. Govedarica, L. Pajewski and X. Derobert, "Automated data extraction from synthetic and real radargrams of district heating pipelines," in *Proc. 9th Inter. Works. on Advanced Ground Penetrating Radar (IWAGPR)*, Edinburgh, 2017, pp. 1-4.

[28] A. Risti, . Bugarinovi, M. Govedarica, L. Pajewski and X. Derobert, "Verification of algorithm for point extraction from hyperbolic reflections in GPR data," in *Proc. 9th Inter. Works. on Advanced Ground Penetrating Radar (IWAGPR)*, Edinburgh, 2017, pp. 1-5.

[29] F. M. Fernandes and J. c. Pais, "Laboratory observation of cracks in road pavements with GPR," *Construction and Building Materials*, vol. 154, pp. 1130-1138, 2017.

[30] A. Benedetto, F. Tosti, L. B. Ciampoli and F. D'Amico, "An overview of ground-penetrating radar signal processing techniques for road inspections," *Signal Processing*, vol. 132, pp. 201-209, 2017.

[31] P. Wiwatrojanagul, R. Sahamitomongkol, S. Tangtermsirikul and N. Khamsemanan, "A new method to determine locations of rebars and estimate cover thickness of RC structures using GPR," *Construction and Building Materials*, vol. 140, pp. 257-273, 2017.

[32] Z. Mechbal and A. Khamlichi, "Determination of concrete rebars characteristics by enhanced post-processing of GPR scan raw data," *NDT&E Intern.*, vol. 89 pp. 30-39, 2017.

[33] C. Warren and A. Giannopoulos, "Experimental and modeled performance of a ground penetrating radar antenna in lossy dielectrics," *IEEE J. Sel. Topics Appl. Earth Obs. Remote Sens.*, vol. 9, no. 1, pp. 29-36, Jan. 2016.

[34] C. W. Chang, C. H. Lin and H. S. Lien, "Measurement radius of reinforcing steel bar in concrete using digital image GPR," *Construction and Building Materials*, vol. 23, pp. 1057-1063, 2009.

[35] V. Utsi and E. Utsi, "Measurement of reinforcement bar depths and diameters in concrete," in *Proc. of 10th Inter. Conf. on Ground Penetrating Radar*, Netherlands, 2004, pp.21-24.

[36] R. Zhan, H. Xie, "GPR measurement of the diameter of steel bars in concrete specimens based on the stationary wavelet transform," *Insight-Non-Destructive Testing and Condition Monitoring* vol. 51, pp. 151-155, 2009.

[37] A. Dolgiy, V. Zolotarev, "Optimal radius estimation for subsurface pipes detected by ground penetrating radar," in *Proc. Inter. Conf. on Ground Penetrating Radar (GPR)*, Columbus Ohio, USA, Vol. 4; 2006.

[38] F. Soldovieri, I. Catapano, P. M. Barone, S. E. Lauro, E. Mattei, E. Pettinelli, G. Valerio, D. Comite, A. Galli, "GPR estimation of the geometrical features of buried metallic targets in testing conditions," *Prog. Electromagn. Res.* vol. 49, pp. 339-362, 2013.

[39] T. Liu, A. Klotzsche, M. Pondkule, H. Vereecken, J. van der Kruk and Y. Su, "Estimation of subsurface cylindrical object properties from GPR full-waveform inversion," in *Proc. Inter. Conf. on Ground Penetrating Radar (GPR)* , Edinburgh, 2017, pp. 1-4.

[40] I. Giannakis, A. Giannopoulos and C. Warren, "Realistic FDTD GPR antenna models optimised using a novel linear/non-linear full waveform inversion," *IEEE Trans. Geosci. Remote Sens.*, Early Access, 2018.

[41] I. Giannakis, A. Giannopoulos, C. Warren and N. Davidson, "Numerical modelling and neural networks for landmine detection using ground penetrating radar," in *Proc. 8th Inter. Works. on Advanced Ground Penetrating Radar (IWAGPR)*, Floremce, pp. 1-4, 2015.

[42] I. Giannakis, A. Giannopoulos and A. Yarovoy, "Model-Based Evaluation of Signal-to-Clutter Ratio for Landmine Detection Using Ground-Penetrating Radar," *IEEE Trans. Geosci. Remote Sens.*, vol. 54, no. 6, pp. 3564-3573, 2016.

[43] K. Yee, "Numerical solution of initial boundary value problems involving Maxwells equations in isotropic media," *IEEE Trans. Antennas Propag.*, vol. 14, no. 3, pp. 302307, May 1966.

[44] A. Taflove and S. C. Hagness, *Computational Electrodynamics, the Finite-Difference Time-Domain Method*, 2nd ed. Norwood, MA, USA: Artech House, 2000.

[45] I. Giannakis and A. Giannopoulos, "A novel piecewise linear recursive convolution approach for dispersive media using the finite-difference time-domain method," *IEEE Trans. Antennas Propag.*, vol. 62, no. 5, pp. 2669-2678, May 2014.

[46] T. Bourdi, J. E. Rhazi, F. Boone and G. Ballivy, "Modelling dielectric-constant values of concrete: an aid to shielding effectiveness prediction and ground-penetrating radar wave technique interpretation," *J. Phys. D: Appl. Phys.*, vol 45, pp. 1-12, 2012.

[47] M. N. Soutsos, J. H. Millard, S. G. Shaw and A. Patterson, "Dielectric properties of concrete and their influence on radar testing," *NDT&E Inter.*, vol. 37, pp. 237-242, 2001.

[48] A. Shaari, S. G. Millard and J. H. Bungey, "Modelling the propagation of a radar signal through concrete as a low-pass filter," *NDT&E Inter.*, vol. 37, pp. 237-242, 2004.

[49] G. A. Meles, J. Van der Kruk, S. A. Greenhalgh, J. R. Ernst, H. Maurer, and A. G. Green, "A new vector waveform inversion algorithm for simultaneous updating of conductivity and permittivity parameters from combination crosshole/borehole-to-surface GPR data," *IEEE Trans. Geosci. Remote Sens.*, vol. 48, no. 9, pp. 3391-3407, 2010.

[50] S. Busch, J. van der Kruk and H. Vereecken, "Improved characterization of fine-texture soils using on-ground GPR full-waveform inversion," *IEEE Trans. Geosci. Remote Sens.*, vol. 52, no. 7, pp. 3947-3958, 2014.

[51] C. Warren and A. Giannopoulos, "Creating finite-difference time-domain models of commercial ground-penetrating radar antennas using Taguchis optimisation method," *Geophysics* , vol. 76, no. 2, pp. G37-G47, Apr. 2011.

[52] S. Kirkpatrick, C. D. Gelatt, and M. P. Vecchi, "Optimization by simulated annealing," *Science* , vol. 220, pp. 671-680, 1983.